The Influence of Bilayer Composition on the Gel to Liquid Crystalline Transition

Ananya Debnath,[†] K. G. Ayappa,*[,†] V. Kumaran,[†] and Prabal K. Maiti[‡]

Department of Chemical Engineering, Centre for Condensed Matter Theory, Department of Physics, Indian Institute of Science, Bangalore 560012, India

Received: February 20, 2009; Revised Manuscript Received: May 6, 2009

We report molecular dynamics simulations of bilayers using a united atom model with explicit solvent molecules. The bilayer consists of the single tail cationic surfactant behenyl trimethyl ammonium chloride (BTMAC) with stearyl alcohol (SA) as the cosurfactant. We study the gel to liquid crystalline transitions in the bilayer by varying the amount of water at fixed BTMAC to SA ratio as well as by varying the BTMAC to SA ratio at fixed water content. The bilayer is found to exist in the tilted, $L_{\beta'}$ phase at low temperatures, and for the compositions investigated in this study, the $L_{\beta'}$ to L_α melting transition occurred in the temperature range 330−338 K. For the highest BTMAC to SA composition (2:3 molar ratio), a diffuse headgroup−water interface is observed at lower temperatures, and an increase in the *d*-spacing occurs prior to the melting transition. This pretransition swelling is accompanied by a sharpening in the water density variation across the headgroup region of the bilayer. Signatures of this swelling effect which can be observed in the alkane density distributions, area per headgroup, and membrane thickness are attributed to the hydrophobic effect. At a fixed bilayer composition, the transition temperature (>338 K) from the $L_{\beta'}$ to L_α transition obtained for the high water content bilayer (80 wt %) is similar to that obtained with low water content (54.3 wt %), confirming that the melting transition at these water contents is dominated by chain melting.

1. Introduction

Bilayers are important constituents of living cell membranes, providing a dynamic interface between the cell and its environment. Membranes are semipermeable, highly selective barriers containing ion channels and pumps which modulate and maintain the osmotic balance across the membrane. Consequently, a fundamental understanding of bilayers and membrane proteins from an atomistic viewpoint is of great biochemical and biophysical interest.[1] A better understanding of the structure and dynamics of membranes and membrane proteins can contribute to the development of pharmaceuticals, anesthetics, and drug-delivery agents. In contrast to lipid bilayers, water−surfactant systems play an important role in detergents, cosmetic formulations, and secondary and tertiary oil recovery processes. Depending on the ratio of the projected hydrophobic core volume to the projected area of the surfactant, water−surfactant systems can arrange into a variety of structures ranging from micelles, bilayers, reverse micelles, and vesicles.[2] Similar to the molecules that constitute lipid bilayers, two tailed surfactants at appropriate compositions can spontaneously assemble to form the bilayer phase in a water−surfactant system. Single tail surfactants can also form bilayers in the presence of an appropriate cosurfactant. Regardless of the specific constituents of the membrane (lipid or surfactant), the bilayer phase displays many generic features and characteristics. Melting from the low temperature gel phase to a high temperature liquid crystalline phase, presence of an intermediate phase such as the tilted and rippled phase, and 1D swelling are some of the common features that have been observed.[3] These features driven by the general hydrophobic effect, often attributed to the formation of complex structures, have been used to build artificial membranes and drug-delivery and biomimetic systems. In this manuscript, we focus on the properties of bilayers made up of surfactants and cosurfactants.

Structural properties of bilayer systems have been investigated by various experimental techniques such as small-angle X-ray scattering (SAXS), small-angle neutron scattering (SANS), Fourier transform infrared spectroscopy (FTIR), and NMR.[4] However, there exists large uncertainties in the structural information obtained from various experimental methods. For example, the area per headgroup for the fluid phase in dipalmitoylphosphatidylcholine (DPPC) bilayers shows wide variation depending on the method used.[4] Phase transitions in the bilayer system have also been studied by differential scanning calorimetry (DSC)[5] and atomic force microscopy.[6] These experimental studies have provided increased insight into the phase behavior of the bilayer structure. However, the majority of these experiments yield one-dimensional information mostly along the bilayer normal such as the bilayer width and electron density profile. Molecular simulations have emerged as an attractive technique to provide microscopic three-dimensional structural information of the bilayer structure as a function of temperature and composition. In this context, computer simulations have played a significant role in elucidating various structure−property relationships of the bilayer system. The models employed in computer simulations range from fully atomistic descriptions to coarse-grained bead−spring descriptions.[7−10] There are a large number of simulation studies of bilayers which optimize the force-field parameters to various structural[11−13] and thermodynamic properties of the bilayer.[14−26] These studies have provided valuable insight into properties such as bilayer width, bending modulus, and density profiles[27] and their dependence on the composition as well as the structure of the surfactant forming the bilayer.[28,29] There have been several studies to show that the coexistence of two lipid phases in cell

* Corresponding author. E-mail: ayappa@chemeng.iisc.ernet.in. Fax: 011-91-80-3600683 (3600085).
† Department of Chemical Engineering.
‡ Centre for Condensed Matter Theory, Department of Physics.

10.1021/jp901551d CCC: $40.75
Published on Web 07/13/2009

membranes is important in performing biological functions like signal transduction,[30,31] protein transport,[30,32] membrane sorting, and possible binding sites for pathogens and toxins.[33,34] In addition, atomistic simulation studies have investigated the effect of additives (such as alcohol, sugar, and cholesterol) as well as surfactant composition on the phase behavior of the lamellar phase.[24,35−37]

Although there is an extensive literature on the phase diagrams that form in water−surfactant systems, there is relatively less information on mixed surfactant systems. In a recent study by Shen et al.,[38] phase transitions from densely packed multilamellar vesicles of cationic surfactant in the presence of salt are observed. Several techniques like Fourier transform infrared spectroscopy (FTIR), turbidity, and viscosity measurements reveal that phase transition of cationic multilamellar vesicles is governed by chain melting in the presence of aqueous solutions at different concentrations of salt and is not influenced by dilution. The phase diagram for mixed cationic and nonionic surfactants was studied using small-angle neutron scattering (SANS).[39,40] For cationic surfactant-rich compositions, the microstructure is in the form of bilamellar or multilamellar vesicles and at higher nonionic surfactant concentrations the lamellar phase is stable. A macroscopic model which takes into account the chain length and chain asymmetry parameter has been used to predict the melting transition in two-component surfactant systems.[41] The proposed model estimates the transition temperature and other structural and thermodynamic quantities which are in excellent agreement with experimental data.

In this manuscript, we carry out a molecular dynamics study of a two-component bilayer having cationic surfactants and cosurfactants. Understanding the dynamic and structural characteristics of these systems is relevant to cosmetics formulations as well as secondary and tertiary oil recovery processes. In contrast to lipid bilayer systems, there are very few molecular dynamics simulations of the mixed-surfactant-based lamellar phases. We consider a bilayer made up of the cationic surfactant behenyl trimethyl ammonium chloride (BTMAC) with stearyl alcohol (SA) as the cosurfactant. Molecular dynamics simulation of the lamellar phase as a function of membrane composition is carried out to gain insight into the role of cosurfactant. We investigate the influence of water content on the melting transition at a fixed membrane composition and study the gel to liquid crystalline transition of the lamellar phase as a function of composition by varying the BTMAC/SA ratio at similar water content. The mechanism of the phase transition for bilayers from a gel to a liquid-crystalline state is directly related to structural changes in the bilayer. As the complex structural dynamics of the bilayers are governed by parameters such as average interfacial area per chains, thickness of bilayer, and degree of disorder in hydrophobic tails, we show how these properties change with temperature and composition. The rest of the paper is organized as follows. In section 2, we give the details of simulation conditions. The results for bilayer melting with different water contents at a fixed composition are given in section 3.1. In section 3.2, we discuss the results for bilayers with different compositions at fixed water content. Finally, in section 4, we give a summary of the main results and conclude.

2. Simulation Details

Simulations are carried out for bilayers made up of the cationic surfactant BTMAC with SA as the cosurfactant. BTMAC is a single tail surfactant with 21 methylene groups having the chemical formula $CH_3-(CH_2)_{21}-N^+Cl^--(CH_3)_3$ (Figure 1a), which is described as $CP_3-(CP_2)_{20}CH_2-LNL-(LC_3)_3$ for the convenience of assigning force-field parameters. SA has 17 methylene groups with the formula $CH_3-(CH_2)_{17}-OH$ (Figure 1b), which is described as $CP_3-(CP_2)_{16}CH_2-OH$. The various bilayer compositions investigated in this manuscript are listed in Table 1. We perform simulations with BTMAC and SA ratios of 1:3 with 80 wt % water (S1), 1:3 with 54.3 wt % water (S2), 1:2 with 50.58 wt % water (S3), and 2:3 with 47.1 wt % water (S4). For all of the systems, S1, S2, S3, and S4, we have investigated the transition from the low temperature gel phase to the liquid crystalline phase by carrying out simulations in the temperature range 283−350 K. The systems S2, S3, and S4 allow us to study the influence of membrane composition on the melting transition, while S1 and S2 assess the influence of water content on the transition.

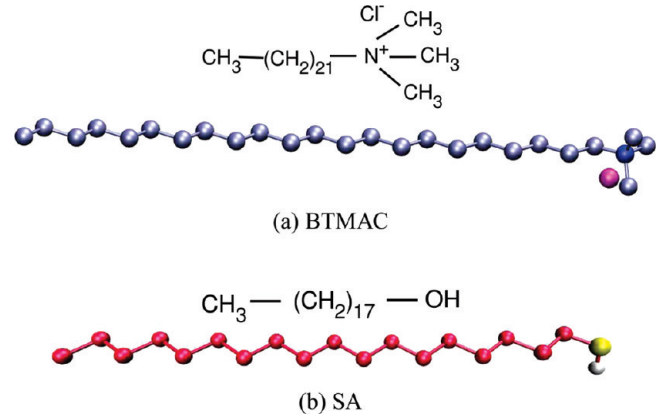

Figure 1. Illustration for (a) behenyl trimethyl ammonium chloride (BTMAC), (b) stearyl alcohol (SA). Color codes: ice blue, BTMAC; blue, nitrogen (N^+) headgroup for BTMAC; magenta, Cl^-; red, SA; yellow, oxygen (O^-) headgroup for SA.

TABLE 1: Number of Behenyl Trimethyl Ammonium Chloride (BTMAC), Stearyl Alcohol (SA), and Water Molecules Used in Different Bilayer Compositions Investigated[a]

	number of molecules			
bilayer	BTMAC	SA	water	NPT (ns)
S1	50	150	13484	25
S2	50	150	4000	25
S3	74	150	4000	25
S4	100	150	4000	25

[a] S1 is the bilayer with 80 wt % water, S2 is the bilayer with 54.3 wt % water, S3 is the bilayer with 50.6 wt % water, and S4 is the bilayer with 47.1 wt % water.

The initial configurations for the bilayers are constructed using the software PACKMOL.[42] The force-field parameters are obtained using GROMOS-87[43] and OPLS[44,45] with the rigid SPC model for water.[46,47] The force-field parameters used in this study are listed in Tables 2 and 3. Energy minimization of the initial structure is carried out with the steepest descent algorithm.[48] Our starting configurations for all of the bilayers, S1, S2, S3, S4, were obtained from configurations equilibrated at 300 K (gel phase) with 0.5−2 ns long NVT runs followed by 3 ns NPT runs. We used the final configuration from this 300 K simulation as the initial configuration for simulations at higher temperatures, 323−350 K. All of the data in the manuscript are reported for NPT simulation run lengths of 25 ns. A similar protocol was used for simulations at 283 K. We monitored the properties such as energy, temperature, and area per headgroup (see Figure S4 in the Supporting Information) during the simulation, which revealed that the run lengths were sufficient

TABLE 2: Force-Field Parameters and Their Literature Source for Behenyl Trimethyl Ammonium Chloride (BTMAC) Described as $CP_3-(CP_2)_{20}CH_2-LNL-(LC_3)_3$

group type	σ (nm)	ϵ (kJ/mol)	q (e)
LC_3	0.3960[a]	0.6067[a]	0.4[b]
LNL	0.3250[c]	0.7113[c]	−0.5[d]
CH_2	0.3905[e]	0.4937[e]	0.3[f]
CP_2	0.3960[g]	0.3800[g]	0.0[g]
CP_3	0.3960[g]	0.5700[g]	0.0[g]

[a] OPLS65.[47] [b] Berendsen et al.[66] [c] OPLS3.[47] [d] Jorgensen et al.[47] [e] OPLS9.[47] [f] Jorgensen.[44] [g] Berger et al.[67]

TABLE 3: Force-Field Parameters and Their Literature Source for Stearyl Alcohol (SA) Described as $CP_3-(CP_2)_{16}CH_2-OH$

group type	σ (nm)	ϵ (kJ/mol)	q (e)
H	0.0000[a]	0.0000[a]	0.435[b]
O	0.3070[a]	0.71128[a]	−0.700[c]
CH_2	0.3905[d]	0.4937[d]	0.265[a]
CP_2	0.3960[e]	0.3800[e]	0.0[e]
CP_3	0.3960[e]	0.5700[e]	0.0[e]

[a] OPLS24.[47] [b] Jorgensen et al.[47] [c] Jorgensen et al.[68] [d] OPLS22.[47] [e] Berger et al.[67]

to equilibrate the system. The time averaged properties reported in this manuscript were obtained from the last 1 ns.

For all of the NPT simulations, the pressure is fixed at 1 bar. The Berendsen thermostat was used to maintain the temperature and the Berendsen semi-isotropic pressure coupling method[49] was used to maintain the zero interfacial tension by using the same magnitudes for the diagonal components of the stress tensor. A time step of 2 fs is used for all simulations. Coulombic and van der Waals interactions were cut off at 1.3 nm. Long-range electrostatic interactions were corrected using the particle-mesh Ewald method with a 0.12 nm grid size. Periodic boundary conditions were applied in all three directions. Trajectories were collected every 2 ps. All simulations were performed with GROMACS-3.3.2.[50,51]

The d-spacing of the bilayer is determined by time averaging the periodic box length in the z-direction which is the direction of the bilayer normal. The membrane thickness is obtained from the peak to peak distance of the BTMAC headgroup (identified by the position of the nitrogen atom) from the time averaged density distribution. The average area per headgroup, a_h, is defined as the area per molecule in the $x-y$ plane of each leaflet in the membrane. In what follows, we refer to the portion of the bilayer that consists of BTMAC and SA as the membrane.

3. Results and Discussion

3.1. Influence of Water Content. Structural changes in the bilayer as a function of temperature are monitored using the order parameter

$$S = \frac{1}{2}\langle 3\cos^2\theta - 1\rangle \qquad (1)$$

where θ is the angle between the C−C bond vector (as we use the united atom model) and the bilayer normal. The bracket denotes a time average as well as an average over the chains in the membrane. The order parameter (S) is computed as a function of the carbon number along the alkyl chain. We note that S can also be obtained experimentally from quadrupole splitting data.[52,53]

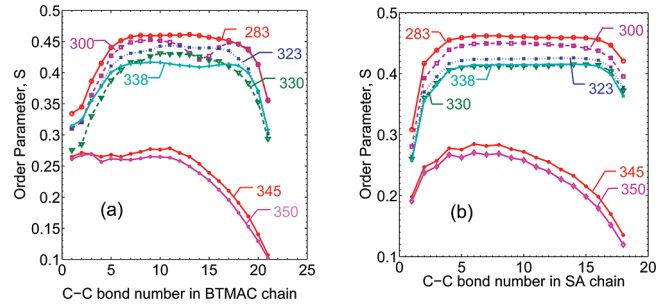

Figure 2. Order parameter for bilayer S1 as a function of the C−C bond along the molecules. The C−C bonds are numbered sequentially beginning from the headgroup: (a) Order parameter for BTMAC at different temperatures from 283 to 350 K. (b) Order parameter for SA at different temperatures from 283 to 350 K. A sharp change in the order parameter is observed above 338 K, and the transition occurs from the $L_{\beta'}$ phase at low temperature to the L_α phase at higher temperature.

The order parameter calculated for both BTMAC and SA for system S1 are illustrated in parts a and b of Figure 2, respectively. The plots illustrate variation in the order parameter for all the C−C bond vectors along the alkyl chain. The bonds are numbered sequentially starting from the headgroup. Order parameters are higher in the middle of the chain than at the ends; however, the value of the order parameter in the central regions of the molecule indicates a tilt angle, θ, ranging between 38° and 40° for temperatures of 283 and 338 K, respectively. At lower temperatures, both the terminal ends of BTMAC have a similar degree of order, as revealed in Figure 2a. The bond order parameters for SA (Figure 2b) indicate that, although the first C−C bond has a lower value of the order parameter when compared with the corresponding value for BTMAC, the overall order in the SA chain is larger both at the headgroup as well as the tail regions of the molecule. This increased order (albeit small) in the SA alkyl chains is attributed to its shorter length and its ability to pack efficiently within the BTMAC molecules of the membrane. As the temperature increases, chains in the bilayer get increasingly disordered, resulting in a lowering of the order parameter. Above 338 K, a sharp decrease in the order parameter is observed. This is the temperature at which the bilayer melts to form the liquid crystalline L_α phase.

Examination of the order parameters for system S2 (Figure S1 in the Supporting Information) revealed similar trends in the order parameter variation with temperature as observed for system S1, indicating that the water content in this range of dilution does not affect the level of order within the membrane. The order parameters for BTMAC and SA averaged over all the C−C bonds are plotted as a function of temperature in parts a and b of Figure 3, respectively, for both systems S1 and S2. As the average order parameter includes all of the bonds in the chain, it gives a more appropriate measure of the onset of disorder within bilayer. On comparing the data for S1 and S2, the transition temperature from the low temperature gel phase to the lamellar phase is relatively unchanged, indicating that the water content plays a small role in the overall enthalpy change associated with the phase transition which is primarily driven by chain melting. As a result, melting occurs at similar temperatures for both S1 and S2.

A second noticeable feature in the order parameter (Figure 3a) is a small decrease, resulting in a local minimum at 330 K. The decrease in the order parameter at 330 K indicates a marginal increase in tilting (about 2°) before the system melts at higher temperatures. Since finite size effects are important in the proximity of the main transition, we carried out simula-

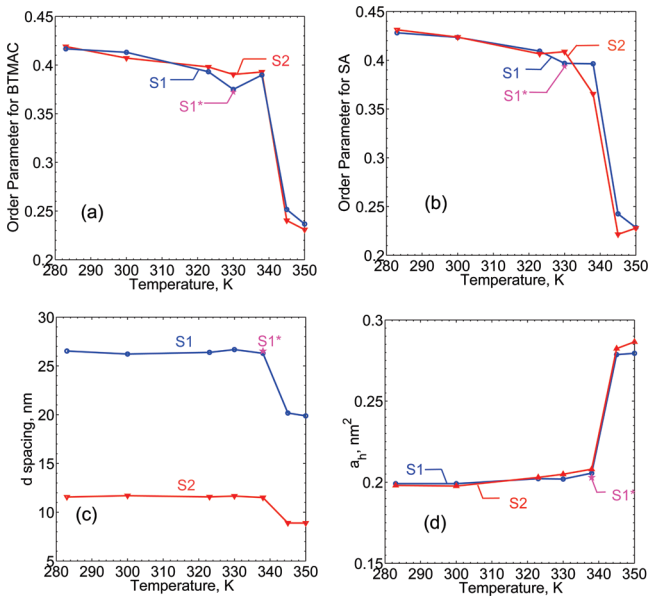

Figure 3. Comparison of chain averaged order parameters (a) BTMAC and (b) SA, bilayer *d*-spacing (c) and area per headgroup (d) for the bilayers S1 and S2. Color codes: blue, S1 high water content; red, S2 low water content; S1*, S1 with larger system size. The order parameters reveal that the melting transition temperatures are invariant at these levels of hydration. At low temperatures, the bilayer is in the tilted $L_{\beta'}$ phase, and above 338 K, the bilayer transforms to the L_α phase. S1* is the result obtained for the S1 bilayer containing 4 times the number of molecules.

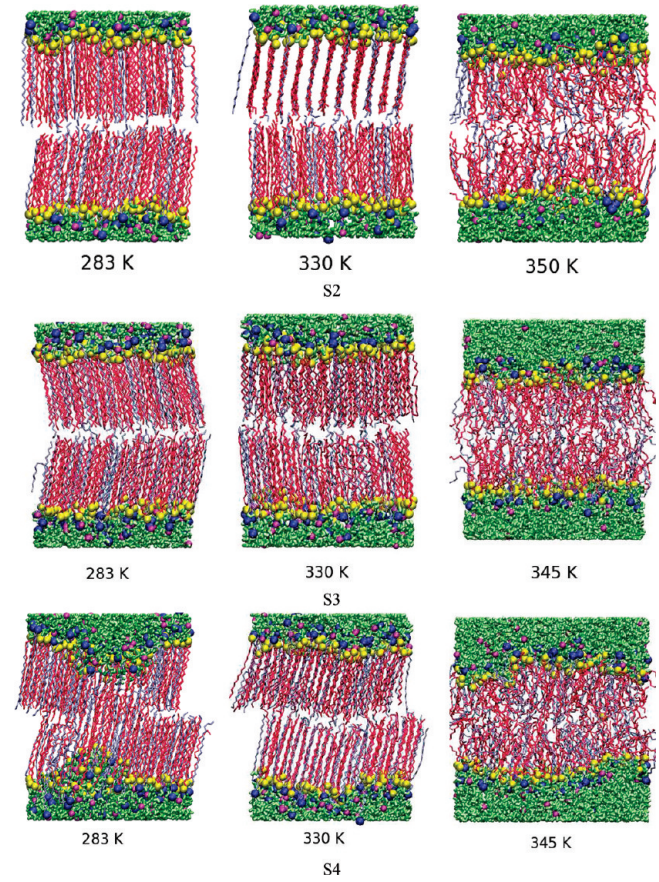

Figure 4. Snapshots for bilayers S2, S3, and S4 at different temperatures: 283, 330, and 345 K. For bilayers S2 and S3, the transition occurs from the tilted $L_{\beta'}$ phase below $T \leq 338$ K to the L_α phase above 338 K. For bilayer S4, the increase in the diffuse nature of the water−headgroup interface is observed at 283 K and the ordering of the hydrocarbon chains occurs at 330 K prior to melting. Color codes: ice blue, behenyl trimethyl ammonium chloride (BTMAC); red, stearyl alcohol (SA); green, water; magenta, Cl^-; yellow, oxygen (O^-) headgroup for SA; blue, nitrogen (N^+) headgroup for BTMAC.

tions with a system that was 4 times as large as S1 (Table 1) in the bilayer plane at 330 K. The value of the order parameter for BTMAC from the large system simulation is 0.37, and the order parameter for SA is 0.39 after a 25 ns run; these values are similar to those obtained with the smaller system. The snapshots for system S2 shown in Figure 4 illustrate the tilted chain configurations at low temperatures, and this is consistent with the relatively low values of the order parameter corresponding to the $L_{\beta'}$ phase. The snapshots clearly reveal two distinct regimes during melting. At low temperatures, the bilayer consists of chains that are fully stretched with no overlap between surfactant and cosurfactant tails from the adjacent leaflets. However, there is a significant overlap of tails from the adjacent leaflets at higher temperature. At low temperatures, we did not observe the formation of the ripple phase in our simulations and perhaps larger simulations are required in order to resolve this phase. Our results indicate that, at lower temperatures before the melting transition, the bilayer is in the $L_{\beta'}$ phase. As the temperature increases, the surfactants as well as cosurfactants undergo melting, and above 350 K, the bilayer is in the L_α phase. Within the resolution of our simulations, melting occurs above 338 K. The calculated melting temperature is in reasonably good agreement with the differential calorimetric (DSC) data obtained at a composition of 30 wt % BTMAC in the membrane (BTMAC + SA) phase (Figure S3 in the Supporting Information) where the melting temperature was reported at 348 K. The composition in the experiment is slightly lower than the 33.2 wt % BTMAC in the membrane phase of the S1 bilayer. The DSC experiments were carried out for a water content (>70 wt % water) substantially higher than the hydration levels of the surfactants. At these high hydration levels, water content is not expected to influence the melting transition.[54]

Parts c and d of Figure 3 illustrate the variation in *d*-spacing and area per headgroup a_h, respectively, for both S1 and S2 as a function of temperature. The increased water content results in a *d*-spacing of 26.53 nm for S1 (Figure 3c) when compared with a *d*-spacing of 11.57 nm for S2 at 283 K. The membrane thickness (Figure 3d) remains relatively unchanged with increasing water content, and the difference in the membrane thickness is within 0.02 nm between systems S1 and S2 at this temperature. Both the *d*-spacing and membrane thickness show a sharp change above 338 K for systems S1 and S2, and this is consistent with the onset of the melting transition, as inferred from the order parameter data (Figure 3a). The area per headgroup a_h for S1 and S2 show similar trends (Figure 3d), and a sharp increase in a_h is observed across the melting transition. The density distributions obtained for the two systems S1 and S2 are compared in parts a and b of Figure 5, respectively, for two temperatures. The density distributions for the two systems are appropriately translated along the bilayer normal to facilitate comparison. At a lower temperature of 300 K which corresponds to the gel phase (Figure 5a), the density distributions do not reveal any differences. This is consistent with the similar values for both the order parameter and the area per headgroup between the two systems. Above the melting temperature, the density distributions compared at 345 K (Figure 5b) show very similar states of order for both the S1 and S2 systems.

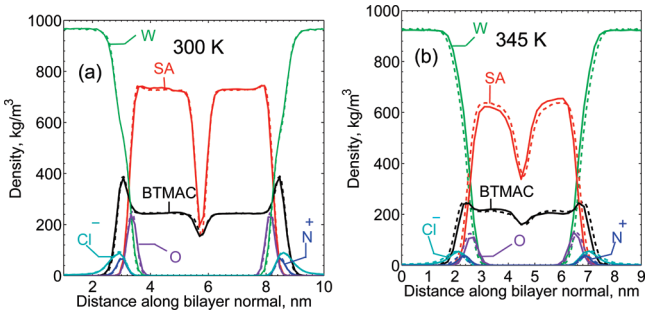

Figure 5. Comparison of layer density distributions for bilayers S1 and S2 at temperatures 300 K (a) and 345 K (b). A similar extent of water penetration is observed at high (S1) and low water content (S2) at both low and high temperatures. The solid lines are data for high water content, S1, and the dashed lines are data for low water content, S2. Color codes: green, water (W); red, stearyl alcohol (SA); black, behenyl trimethyl ammonium chloride (BTMAC); blue, nitrogen (N^+) headgroup for BTMAC; purple, oxygen (O^-) headgroup for SA; cyan, chloride ion (Cl^-).

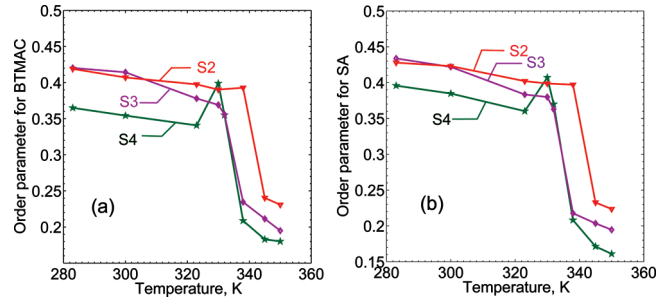

Figure 6. Chain averaged order parameters for (a) BTMAC and (b) SA for bilayer compositions S2, S3, and S4. Color codes: red, S2; magenta, S3; green, S4. Increasing the BTMAC content is seen to decrease the transition temperature by about 8 K. At the highest BTMAC content (S4), the *d*-spacing shows a sharp increase indicative of increased order in the alkane tails prior to the melting transition.

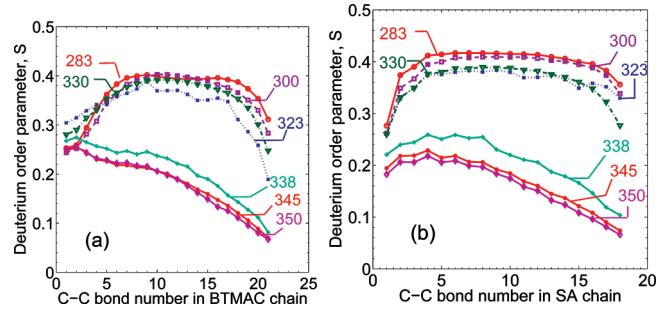

Figure 7. Order parameter for bilayer S4 as a function of the C−C bond along the molecules. The C−C bonds are numbered sequentially beginning from the headgroup: (a) Order parameter for BTMAC at different temperatures from 283 to 350 K. (b) Order parameter for SA at different temperatures from 283 to 350 K. A sharp change in the order parameter is observed above 330 K, and the transition occurs from the $L_{\beta'}$ phase at low temperature to the L_α phase at higher temperature. Most importantly, unlike the other order parameters for bilayers S1, S2, and S3, the order parameter for bilayer S4 increases as the temperature is increased from 323 to 330 K.

3.2. Influence of Membrane Composition and Pretransition Swelling. In this section, we compare the results obtained for systems S2, S3, and S4, i.e., bilayers with similar water content, but with different membrane compositions obtained by varying the BTMAC to SA ratio (Table 1). The order parameters in Figure 6 reveal that the degree of disorder increases as the BTMAC concentration in the bilayer is increased from S2 to S4 (33.3−49.9 wt %). The low temperature $L_{\beta'}$ phase that is formed possesses a greater degree of tilt in the alkyl chains as the BTMAC fraction is increased. From the values of the BTMAC order parameter at low temperatures, the tilt increased by about 2° going from S2 to S4. A distinct lowering of the melting transition temperature, T_m, is observed from S2 to S3. Bilayer S3 melts above a temperature of 330 K, which is 8 K lower than the melting temperature of 338 K for S2. We do not observe a change in the melting temperature between S3 and S4. Additional simulations at finer temperature intervals in the proximity of the transition did not reveal any difference in the melting temperatures. Similar to the trends observed for S2, the order parameters for SA (Figure 6b) are higher than the order parameter obtained for BTMAC. This trend is also evident from the order parameters obtained for individual C−C bonds along the molecule for bilayer S3 (Figure S2 in the Supporting Information). The most significant observation is the presence of a new feature for bilayer S4 where the order parameter shows a sharp increase above 320 K prior to the main melting transition. This trend was not observed at the lower BTMAC compositions. The order parameter variation along the C−C bonds is illustrated in Figure 7 for bilayer S4. The increase in order parameter along the alkyl chains as the temperature is increased from 323 to 330 K is distinctly observed for BTMAC and to a lesser extent for SA. These results indicate that in the pretransition regime an increase in temperature increases the chain order in the membrane. We discuss the reasons behind this anomalous trend below.

Figure 8 illustrates the *d*-spacing, a_h, and the membrane thickness as a function of temperature for systems S2, S3, and S4. Increasing the BTMAC concentration in the membrane reduces the *d*-spacing in the bilayers, and a decrease of 2.3 nm is observed at 283 K going from S2 to S4. At the same temperature, the change in the membrane thickness is relatively small, reducing by 0.2 nm from S2 to S4 (Figure 8c). Since the amount of water is similar for all three systems, the reduction in *d*-spacing compensates for the increase in a_h in order to maintain a constant water density in the bilayer. We note that the average lateral area of the simulation box is different for all three cases increasing from S2 to S4. This is partly due to the increase in the number of molecules within the membrane. The point at which the melting transition occurs is observable in all three quantities, and the reduction in the melting temperature for S3 and S4 when compared with S2 is very distinct. The *d*-spacing and membrane thickness decrease across the transition, and a_h increases across the transition. Chain melting results in an increase in the projected area of the hydrophobic region to compensate for the increased area per headgroup. Hence, the change in the area per headgroup is a sensitive indicator of the transition. The areas per headgroup for systems S2 and S3 are similar for temperatures up to 300 K. Above 300 K, the increase in a_h for S3 is more rapid when compared with S2 and the sharp increase above 300 K is a clear signature of the melting transition; increasing the BTMAC concentration in the membrane reduces the transition temperature by 8 K.

In the case of S4, the *d*-spacing increases as the temperature is increased toward the main transition (Figure 8a). This behavior is not observed in the *d*-spacing for S1 (Figure 3c), S2, and S3, as a function of temperature. The increase in *d*-spacing is observed between 323 and 330 K for S4 which is below the main transition, and hence, we refer to this as the pretransition swelling. In the same temperature range, a_h decreases and the membrane thickness is seen to increase. These anomalous changes are associated with the observed increase in the order parameters for S4 (Figure 7) at 330 K. The reasons

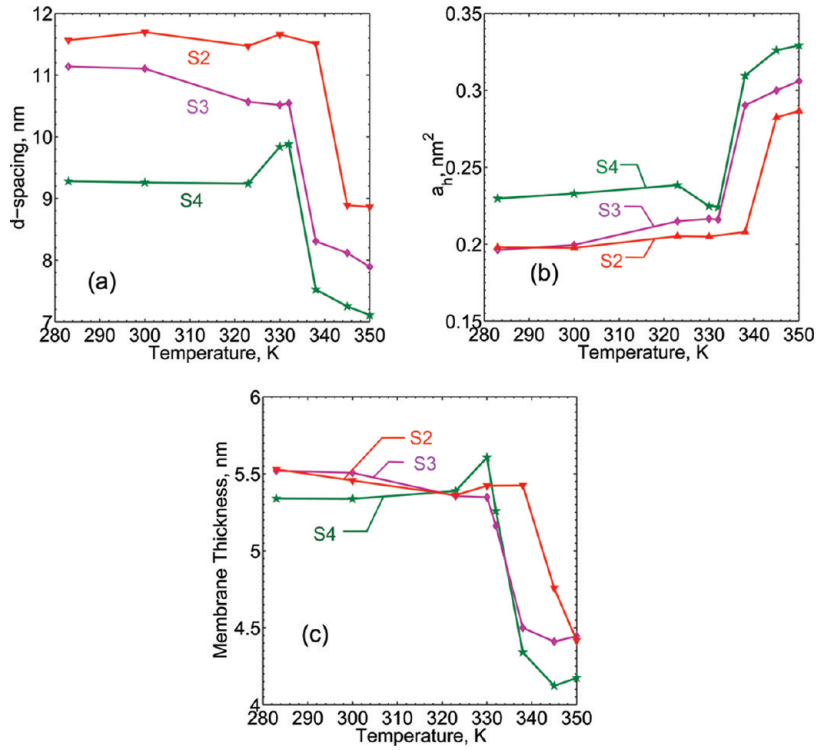

Figure 8. Variation in (a) *d*-spacing, (b) area per headgroup, and (c) membrane thickness as a function of temperature for bilayers S2, S3, and S4. Color codes: red, S2; magenta, S3; green, S4. A decrease in the melting transition is observed going from S2 to S3. For composition S4, the *d*-spacing and membrane thickness increase, leading to a swelling of the lamellar phase prior to the main melting transition. This swelling is accompanied by a decrease in a_h for bilayer S4. The swelling is a result of increased order (Figure 7) in the chains as the temperature is raised. This results in expulsion of water from the membrane, leading to swelling as observed in the *d*-spacing data (part a).

behind these anomalous trends are best elucidated with the aid of the density distributions for S4 (Figure 9) and snapshots (Figure 4). At 283 K, the density distribution reveals a diffuse water interface in contrast to the relatively sharp interface observed for S1 and S2 (Figure 5) at lower temperature, suggesting increased water hydration at the bilayer interface for S4. The oxygen (SA) and the nitrogen (BTMAC) peaks are broader and flatter, and this is accompanied by a diffuse Cl^- ion distribution. The density distribution shows a significantly looser packed headgroup configuration in the case of S4, when compared with the other membrane compositions. This diffuse distribution of head groups is also clearly visible in the snapshots for bilayer S4 (Figure 4). As the temperature is increased, the extent of water association and the diffuse nature of the interface is unaltered until 323 K (Figure 9b). At 330 K, a distinct sharpening in the density distributions occurs and this is clearly observed in Figure 9c. The increased order is observed not only for the N^+ and O head groups and Cl^- counterions but in the alkyl chains as well. The net effect results in a sharpening of the water density as the temperature is increased. The expulsion of water from the membrane at 330 K is consistent with the accompanied increase in the *d*-spacing and membrane thickness (Figure 8a and c, respectively) and the concomitant decrease in a_h (Figure 8b). At 338 K (Figure 9d), the bilayer is in the L_α phase and the alkyl chains are significantly more disordered, as observed from the lower chain density. However, water penetration into the bilayer is prevented by chain melting, resulting in a decrease in the membrane thickness, a generic phenomenon associated with the melting transition in bilayers.

The increased water association with the membrane for the S4 bilayer in the gel phase at the lower temperatures is due to the greater hydrophilicity associated with the bulkier BTMAC amine headgroup. The diffuse nature of the water−headgroup interface increases the association of water with the hydrocarbon tails of the surfactant. This results in a diffuse water−surfactant interface observed in both the density distributions (Figure 9) and snapshots (Figure 4). This situation persists for temperatures up to $T = 323$ K, above which the swelling is observed. It is possible that the increased hydration and consequent water penetration into the bilayer are signatures of the composition lying in the proximity of a phase boundary. In order to check this possibility, we carried out a simulation with a 1:1 (BTMAC:SA) composition. The bilayer was found to be stable after a 25 ns NPT simulation and similar topological features of the S4 composition were observed. We point out that identifying phase boundaries is complicated by inherent finite size effects which are computationally prohibitive to probe within the all-atom simulation framework and suitable coarse-grained methods are usually preferred.[8] As an added check, we carried out a simulation at $T = 283$ K, with an initial configuration corresponding to $T = 338$ K. The resulting *d*-spacing and degree of water penetration as observed in the density distribution at 283 K were unaltered. In all of our compositions studied, we did not observe any tendency for lateral phase separation in the bilayer as a function of composition. This conclusion was based on examining in-plane snapshots of the head groups.

We attribute the increased order observed in the hydrocarbon tails and the resulting increase in the *d*-spacing prior to the melting transition to the hydrophobic effect.[55,56] The swelling and associated increased order in the membrane is observed in a small temperature window of 323 K < T < 330 K. The hydrophobic effect is associated with the increased attraction between hydrophobic (nonpolar) entities in water with an increase in temperature. Hence, the depth of the potential of mean force between two nonpolar solutes in water is seen to increase with temperature up to a critical temperature. This

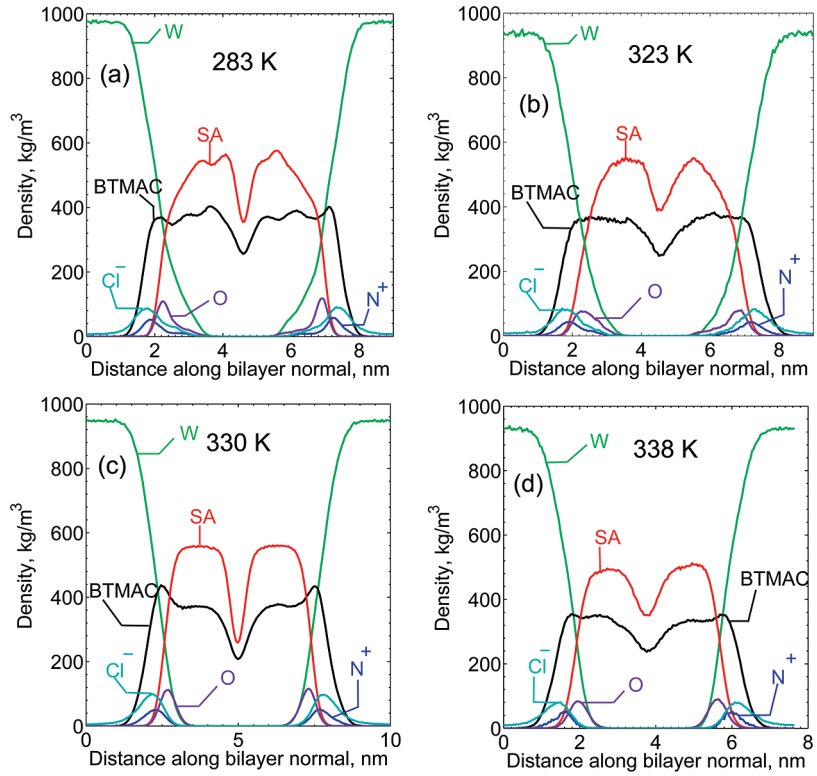

Figure 9. Layer density distributions for bilayer S4 at different temperatures illustrating the sharpening of the water−bilayer interface as the temperature is increased from 283 to 330 K. Color codes: green, water (W); red, stearyl alcohol (SA); black, BTMAC; blue, nitrogen (N^+) headgroup for BTMAC; purple, oxygen (O^-) headgroup for SA; cyan, chloride ion (Cl^-). The density distributions indicate increased water penetration and diffuse density distributions at the water−headgroup interface at the lower temperatures 283 and 323 K. At 330 K, where an increase in the *d*-spacing (Figure 8a) and order parameter (Figure 7) are observed, the density distributions reveal increased order in the membrane. At 338 K, the bilayer is in the L_α phase.

increased interaction between nonpolar solutes is termed as the hydrophobic effect and is primarily driven by the net entropy gained by water as a result of this association. This effect has been attributed to the driving force behind self-assembling systems and protein folding.[57] The increased order between the alkyl chains for the S4 bilayer as the temperature is increased from 323 K displays characteristics that are qualitatively similar to those associated with the hydrophobic effect. We note that the bilayer expansion observed in our simulations is different from the anomalous swelling phenomenon that has been extensively investigated for the lamellar phase.[58,59] Unlike the effect reported in this manuscript, the anomalous swelling is observed in the L_α phase and is associated with the increase in *d*-spacing as the temperature is lowered in the L_α phase. In contrast, the increased chain order observed in this study occurs below the main melting transition while the bilayer is in the gel phase. Part of the contribution to the swelling observed for bilayer S4 in the pretransition region arises from the untilting of chains. However, the increase in membrane thickness due to untilting is 2.7 Å when compared with the increase in *d*-spacing which is 5.6 Å (Figure 8a and c). Hence, the increase in the membrane thickness accounts for about 51.8% of the observed increase in *d*-spacing. Untilting observed in the pretransition region, however, is attributed to the hydrophobic effect, inducing increased ordering between the hydrocarbon chains, leading to a decrease in the association of water within the membrane.

It is possible that the low temperature phase for the S4 bilayers prior to the onset of swelling is in the rippled phase ($P_{\beta'}$). However, additional analysis is required to make a definitive conclusion on the existence of the $P_{\beta'}$ phase for temperatures below the swelling anomaly. We point out however that the extensive literature on the $P_{\beta'}$ phase[60−62] indicates that the $P_{\beta'}$ phase occurs as a pretransition phase and directly transforms to the L_α phase upon heating. It has also been suggested that the presence of ripples on the membrane initiates grain boundary defects leading to the melting of the bilayer.[62] In contrast, our study conclusively shows that the pretransition phase associated with the swelling anomaly observed here is a well ordered $L_{\beta'}$ phase. A snapshot at 330 K shown in Figure 4 for S4 illustrates a highly ordered bilayer. Simulations with a 4 times larger system at 330 K (for 16 ns) also revealed similar features, and neither interdigitation or evidence of rippling was observed.

4. Summary and Conclusion

We have studied the structural changes in bilayers that occur across the melting transition with particular emphasis on the influence of water content and membrane composition on the transition. Water plays an important role in stabilizing the bilayer phase by screening the electrostatic repulsion between the surfactant and cosurfactant head groups that form the membrane as well as hydrating the hydrophilic head groups. Our simulations indicate that, once there is sufficient water to hydrate the head groups and stabilize the bilayer, water does not influence the melting transition temperature. Systems S1 and S2 have similar membrane compositions; however, S1 has a *d*-spacing of 26.53 nm when compared with the *d*-spacing for S2 which is 11.57 nm at 283 K. The variation in the area per headgroup and order parameters indicate that the transition temperature between S1 and S2 occurs above 338 K and there is little influence of the added water content at a fixed membrane

composition. This is consistent with the view that the melting transition is primarily driven by chain melting.

In all of the compositions investigated, the low temperature phase corresponds to the $L_{\beta'}$ phase where the surfactant and cosurfactant tails are tilted at an angle to the bilayer normal. The magnitude of the tilt or the presence of the tilted ($L_{\beta'}$) phase arises from the mismatch between the area per headgroup a_h and the projected area of the alkyl chains. When this mismatch is small, the alkyl chains align along the bilayer normal, giving rise to the L_β phase. From the BTMAC order parameter, the low temperature phase is characterized by a tilt angle of 38° for the S2 bilayer. In all of the systems investigated, we observe that SA which serves as the cosurfactant in stabilizing the membrane has a marginally higher degree of order within the membrane as inferred from the order parameter and density distribution data.

Increasing the BTMAC concentration at a fixed water content has some interesting consequences on the bilayer stability and melting characteristics. The dominant effect due to increasing the BTMAC concentration is the greater area per headgroup in the membrane, which leads to an increase in the tilt angle to 40° for the $L_{\beta'}$ phase in system S4. Tilting not only compensates for the increased free volume for the chain but optimizes the packing and resulting van der Waals interaction between the alkyl chains. This is qualitatively similar to the tilting observed with self-assembled monolayers on solid substrates[63] as well as Langmuir monolayers.[64,65]

A novel finding in this study is the anomalous trends observed with increasing temperature as the BTMAC to SA ratio is increased. In contrast to the monotonic decrease in order parameter across the $L_{\beta'}$ to L_α transition, we observe an increase in the order parameter prior to the main transition. This situation is observed for the highest BTMAC to SA ratio (S4) membrane investigated. This improved hydrocarbon chain order as the temperature is increased ($T < T_m$) leads to a sharpening of the headgroup−water interface. This trend is clearly captured by the increase in the *d*-spacing and membrane thickness as well as a decrease in the area per headgroup, a_h. We attribute this anomalous pretransition swelling with increasing temperature to the hydrophobic effect, which is associated with the increased attraction between hydrocarbon tails, leading to an expulsion of water from the membrane. Although the increased order for the S4 bilayer has the correct temperature dependence associated with the hydrophobic effect, a more detailed thermodynamic analysis of the enthalpic and entropic changes would be required to make a more definitive conclusion. We are currently pursuing these calculations.

Acknowledgment. This work was carried out with a research grant from P & G Corporation USA. We would like to thank Foram Thakkar, Bruce Murch, Pierre Verstraete, and Gaurav Porwal for many useful technical discussions during the progress of the work. We also thank A. V. Raghunathan for discussions related to the anomalous swelling effect.

Supporting Information Available: Figures showing order parameters for the bilayers S2 and S3 as a function of the C−C bond along the molecule, differential scanning calorimetry data for a membrane containing 30 wt % BTMAC, and area per head group of the bilayer S1 plotted against time for all of the temperatures. This material is available free of charge via the Internet at http://pubs.acs.org.

References and Notes

(1) Moore, P. B.; Lopez, C. F.; Klein, M. L. *Biophys. J.* **2001**, *81*, 2484–2494.
(2) Israelachvili, J. N. *Intermolecular and surface forces*; Academic Press: San Diego, CA, 1992.
(3) Evans, D. F.; Wennerstrom, H. *The Colloidal Domain Where Physics, Chemistry, Biology and Technology Meet*; VCH: New York, 1994.
(4) Nagle, J. F.; Tristram-Nagle, S. *Biochim. Biophys. Acta* **2000**, *1469*, 159–195.
(5) Naumann, C.; Brumm, T.; Bayerl, T. M. *Biophys. J.* **1992**, *63*, 1314–1319.
(6) Leonenko, Z. V.; Finot, E.; Ma, H.; Dahms, T. E. S.; Cramb, D. T. *Biophys. J.* **2004**, *86*, 3783–3793.
(7) Goetz, R.; Lipowsky, R. *J. Chem. Phys.* **1998**, *108*, 7397.
(8) Maiti, P.; Lansac, Y.; Glaser, M. A.; Clark, N. A.; Rouault, Y. *Langmuir* **2002**, *18*, 1908.
(9) Rekvig, L.; Hafskjold, B.; Smit, B. *J. Chem. Phys.* **2004**, *120*, 4897.
(10) Marrink, S. J.; Risselada, H.; Yefimov, S.; Tieleman, D.; de Vries, A. *J. Phys. Chem. B* **2007**, *111*, 7812–7824.
(11) Nielsen, S. O.; Lopez, C. F.; Ivanov, I.; Moore, P. B.; Shelley, J. C.; Klein, M. L. *Biophys. J.* **2004**, *87*, 2107–2115.
(12) Koubi, L.; Saiz, L.; Tarek, M.; Scharf, D.; Klein, M. L. *J. Phys. Chem. B* **2003**, *107*, 14500–14508.
(13) Saiz, L.; Klein, M. L. *Acc. Chem. Res.* **2002**, *35*, 482–489.
(14) Egberts, E.; Marrink, S. J.; Berendsen, H. J. C. *Eur. Biophys. J.* **1994**, *22*, 423–436.
(15) Chiu, S. W.; Clark, M.; Balaji, V.; Subramaniam, S.; Scott, H. L.; Jakobsson, E. *Biophys. J.* **1995**, *69*, 1230–1245.
(16) Marrink, S. J.; Lindahl, E.; Edholm, O.; Mark, A. E. *J. Am. Chem. Soc.* **2001**, *123*, 8638–8639.
(17) Anzo, C.; de Vries, A. H.; Hltje, H.-D.; Tieleman, D. P.; Marrink, S.-J. *J. Phys. Chem. B* **2003**, *107*, 9424–9433.
(18) Knecht, V.; Mark, A.; Marrink, S. *J. Am. Chem. Soc.* **2006**, *128*, 2030–2034.
(19) Nielsen, S. O.; Klein, M. L. *Bridging the Time Scales: Molecular Simulations for the Next Decade*; Springer: Berlin, 2002.
(20) Tu, K.; Tobias, D. J.; Klein, M. L. *Biophys. J.* **1995**, *69*, 2558–2562.
(21) Gurtovenko, A. A.; Patra, M.; Karttunen, M.; Vattulainen, I. *Biophys. J.* **2004**, *86*, 3461–3472.
(22) Sammalkorpi, M.; Karttunen, M.; Haataja, M. *J. Phys. Chem. B* **2007**, *111*, 11722–11733.
(23) Bennun, S. V.; Longo, M. L.; Faller, R. *J. Phys. Chem. B* **2007**, *111*, 9504–9512.
(24) Faller, R.; Marrink, S. J. *Langmuir* **2004**, *20*, 7686–7693.
(25) Essmann, U.; Perera, L.; Berkowitz, M. L. *Langmuir* **1995**, *11*, 4519–4531.
(26) Essmann, U.; Berkowitz, M. L. *Biophys. J.* **1999**, *76*, 2081–2089.
(27) de Vries, A. H.; Mark, A. E.; Marrink, S. J. *J. Phys. Chem. B* **2004**, *108*, 2454–2463.
(28) Klein, M. L.; Shinoda, W. *Science* **2008**, *321*, 798–800.
(29) Shinoda, W.; Devane, R.; Klein, M. L. *Mol. Simul.* **2007**, *33*, 27–36.
(30) Brown, D. A.; London, E. *Annu. Rev. Cell Dev. Biol.* **1998**, *14*, 111–136.
(31) Simons, K.; Toomre, D. *Nat. Rev. Mol. Cell Biol.* **2001**, *1*, 31–41.
(32) Simons, K.; Ikonen, E. *Nature* **1997**, *387*, 569–572.
(33) Herreros, J.; Ng, T.; Schiavo, G. *Mol. Biol. Cell* **2001**, *12*, 2947–2960.
(34) Marrink, S. J.; Risselada, J.; Mark, A. E. *Chem. Phys. Lipids* **2005**, *135*, 223–224.
(35) Patra, M.; Salonen, E.; Terama, E.; Vattulainen, I.; Faller, R.; Lee, B. W.; Holopainen, J.; Karttunen, M. *Biophys. J.* **2006**, *90*, 1121–1135.
(36) Shi, Q.; Voth, G. A. *Biophys. J.* **2005**, *89*, 2385–2394.
(37) Leekumjorn, S.; Sum, A. K. *Biophys. J.* **2006**, *90*, 3951–3965.
(38) Shen, Y.; Hao, J.; Hoffmann, H.; Wu, Z. *Soft Matter* **2008**, *4*, 805–810.
(39) Tucker, I.; Penfold, J.; Thomas, R. K.; Grillo, I.; Barker, J. G.; Mildner, D. F. R. *Langmuir* **2008**, *24*, 7674–7687.
(40) Tucker, I.; Penfold, J.; Thomas, R. K.; Grillo, I.; Mildner, D. F. R.; Barker, J. G. *Langmuir* **2008**, *24*, 10089–10098.
(41) Chen, L.; Johnson, M. L.; Biltonen, R. L. *Biophys. J.* **2001**, *80*, 254–270.
(42) Martínez, J. M.; Martínez, L. *J. Comput. Chem.* **2003**, *24*, 819–825.
(43) van der Spoel, D.; Lindahl, E.; Hess, B.; van Buuren, A. R.; Apol, E.; Meulenhoff, P. J.; Tieleman, D. P.; Sijbers, A. L. T. M.; Feenstra, K. A.; van Drunen, R.; Berendsen, H. J. C. *Gromacs User Manual version 3.3*; The Netherlands, 2006.
(44) Jorgensen, W. L. *J. Phys. Chem.* **1986**, *90*, 6379–6388.
(45) Kaminski, G. A.; Friesner, R. A.; Tirado-Rives, J.; Jorgensen, W. L. *J. Phys. Chem. B* **2001**, *105*, 6474–6487.

(46) Mark, P.; Nilsson, L. *J. Phys. Chem. A* **2001**, *105*, 9954–9960.
(47) Jorgensen, W. L.; Tirado-Rives, J. *J. Am. Chem. Soc.* **1988**, *110*, 1657–1666.
(48) Leach, A. R. *Molecular modelling: principles and applications*; Pearson Education Limited: Essex, England, 2001.
(49) Berendsen, H. J. C.; Postma, J. P. M.; van Gunsteren, W. F.; DiNola, A.; Haak, J. R. *J. Chem. Phys.* **1984**, *81*, 3684–3690.
(50) Berendsen, H. J. C.; van der Spoel, D.; van Drunen, R. *Comput. Phys. Commun.* **1995**, *91*, 43–56.
(51) Lindahl, E.; Hess, B.; van der Spoel, D. *J. Mol. Model.* **2001**, *7*, 306–317.
(52) Feller, S. E.; Venable, R. M.; Pastor, R. W. *Langmuir* **1997**, *13*, 6555–6561.
(53) Pastor, R. W.; Venable, R. M.; Feller, S. E. *Acc. Chem. Res.* **2002**, *35*, 438–446.
(54) Feller, S. E.; Yin, D.; Pastor, R. W.; MacKerell, A. D. *Biophys. J.* **1997**, *73*, 2269–2279.
(55) Widom, B.; Bhimalapuram, P.; Koga, K. *Phys. Chem. Chem. Phys.* **2003**, *5*, 3085–3093.
(56) Chandler, D. *Nature* **2005**, *437*, 640–647.
(57) Zhou, R.; Huang, X.; Margulis, C. J.; Berne, B. J. *Science* **2009**, *305*, 1605–1609.
(58) Korreman, S. S.; Posselt, D. *Eur. Phys. J. E* **2000**, *1*, 87–91.
(59) Pabst, G.; Katsaras, J.; Raghunathan, V. A.; Rappolt, M. *Langmuir* **2003**, *19*, 1716–1722.
(60) de Vries, A. H.; Yefimov, S.; Mark, A. E.; Marrink, S. J. *Proc. Natl. Acad. Sci. U.S.A.* **2005**, *102*, 5392–5396.
(61) Sun, W. J.; Nagle, S. T.; Suter, R. M.; Nagle, J. F. *Proc. Nat. Acad. Sci. U.S.A.* **1996**, *93*, 7008–7012.
(62) Lenz, O.; Schmid, F. *Phys. Rev. Lett.* **2007**, *98*, 058104-1–058104-4.
(63) Ulman, A. *Chem. Rev.* **1996**, *96*, 1533–1554.
(64) Nielsen, S. O.; Lopez, C. F.; Moore, P. B.; Shelley, J. C.; Klein, M. L. *J. Phys. Chem. B* **2003**, *107*, 13911–13917.
(65) Prathima, N.; Harini, M.; Rai, N.; Chandrashekara, R. H.; Ayappa, K. G.; Sampath, S.; Biswas, S. K. *Langmuir* **2005**, *21*, 2364–2374.
(66) Berendsen, H.; Egberts, E.; Marrink, S.; Ahlstrom, P. *Membrane Proteins: Structures, Interactions and Models*; Kluwer Academic Publishers: Amsterdam, The Netherlands, 1992.
(67) Berger, O.; Edholm, O.; Jähnig, F. *Biophys. J.* **1997**, *72*, 2002–2013.
(68) Jorgensen, W. L. *J. Phys. Chem.* **1986**, *90*, 1276–1284.

JP901551D